INTEGRATION the VLSI journal 58 (2017) 518–527

Contents lists available at ScienceDirect

INTEGRATION, the VLSI journal

journal homepage: www.elsevier.com/locate/vlsi

Dynamic electromigration modeling for transient stress evolution and recovery under time-dependent current and temperature stressing☆

Xin Huang[a,*], Valeriy Sukharev[b], Taeyoung Kim[c], Sheldon X.-D. Tan[a]

[a] Department of Electrical and Computer Engineering, University of California at Riverside, Riverside, CA 92521, USA
[b] Mentor Graphics Corporation, Fremont, CA 94528, USA
[c] Department of Computer Science and Engineering, University of California at Riverside, Riverside, CA 92521, USA

ARTICLE INFO

Keywords:
Electromigration
Hydrostatic stress
Recovery
Time-to-failure

ABSTRACT

Electromigration (EM) has been considered to be the dominant back end of line (BEOL) reliability issue for current and future VLSI technologies. Current EM reliability analysis is overloaded by over-conservative and simplified EM models. Particularly the transient recovery effect in the EM-induced stress evolution kinetics has never been modeled properly in all the existing analytical EM models. In this article, we propose a new physics-based dynamic compact EM model, which for the first time, can accurately predict the transient hydrostatic stress recovery effect in a confined metal wire. The evolution of preexisted void volume and the corresponding metal line resistance change can be further derived based on the stress evolution. The new dynamic EM model is based on the direct analytical solution of one-dimensional Korhonen's equation with load driven by any unipolar or bipolar current waveforms under varying temperature. We show that the EM recovery effect can be quite significant even under unidirectional current loads. This recovery/healing process is sensitive to temperature, and higher temperatures lead to faster and more complete recovery. Such effect can be further exploited to extend the lifetime of the interconnect wires if the chip current or power can be properly regulated and managed. As a result, the new dynamic EM model can be incorporated with existing dynamic thermal/power/reliability management and optimization approaches, devoted to reliability-aware optimization at multiple system levels (chip/server/rack/data centers). Presented results show that the proposed EM model agrees very well with the numerical analysis results under any time-varying current density and temperature profiles.

1. Introduction

Electromigration is the primary failure source for VLSI interconnects. As technology advances into the sub-10 nm regime with FinFET devices, EM induced failure is projected to get even worse due to the increasing current densities and elevated temperature thanks to shrinking interconnect geometries and high temperature around the fins in the FinFET transistors. EM driven design rules based on the worst-case conditions will lead to the very conservative overdesigns, which can significantly increase the chip areas, powers and costs [1]. Lack of the accurate EM models, which can be used at the circuit and system levels for optimizing the EM-induced chip lifetime, limits our capability of properly handling the EM reliability.

EM induced degradation of electric resistance in a variety of test structures is traditionally monitored by applying the DC stressing. A majority of proposed physical models describing the EM phenomenon have also assumed the DC load. At the same time all semiconductor integrated circuit (IC) chips operate with time-dependent, for example AC or pulse, electric currents. Today's multi/many-core microprocessors are working on different performance states and are the subject for dynamic power/thermal management schemes. At the server and rack and even data center levels, many low power techniques such as the KnightShift architecture for scaling energy proportionality scheme using hybrid performance servers [2] and the big.LITTLE technology from ARM at the chip level can create dynamic power, and, hence, across-die temperature profiles [3]. Such dynamic power/energy scheduling and provisioning could result in large variations in current density and temperature, which can have huge impacts on the EM-induced stress evolution in interconnect wires and, thus, effect the failure development.

One important transient behavior in EM stress evolution is the recovery effect shown in Fig. 1. It refers to the stress relaxation or

☆ This work is supported in part by NSF grant under No. CCF-1255899, in part by No. CCF-1527324, in part by Semiconductor Research Corporation (SRC) Grant under No. 2013-TJ-2417.

* Corresponding author.
E-mail addresses: xhuan009@ucr.edu (X. Huang), stan@ece.ucr.edu (S.X.-D. Tan).

http://dx.doi.org/10.1016/j.vlsi.2016.10.007
Received 30 April 2016; Received in revised form 14 September 2016; Accepted 12 October 2016
Available online 12 November 2016

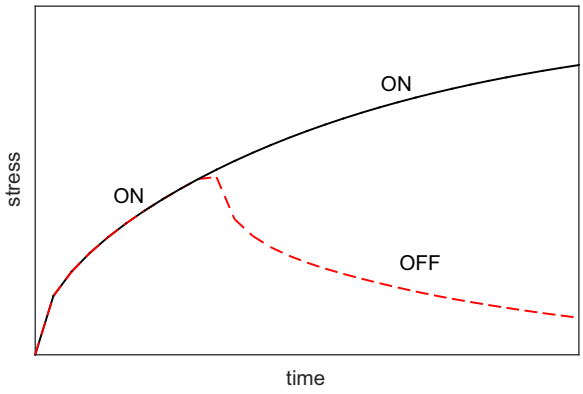

Fig. 1. Stress relaxation (EM recovery) when current is switched-off.

decreasing in the metal line, which occurs when the current is switched-off. It can be considered as the healing process extending the lifetime of interconnects. Manifestation of the recovery of EM-induced stress buildup has been observed and reported in many papers [4–7]. This phenomenon is very visible when the wire is stressed by symmetric bi-directional (bipolar) pulse current waveforms. It becomes less obvious when the current waveforms are unidirectional (unipolar) characterized by the high frequencies (larger than kHz) [6,7]. However, a lot of experimental works have found that when the frequencies of current waveforms are small enough (its period is about 100 s or longer), we can still see significant EM recovery, which extends the lifetime of the stressed wire [5]. Such low frequency power/temperature patterns are typical today due to the proposed low power techniques at chip/server/rack levels, which can be operated at the time scale of minutes and hours. Emerging dark silicon also requires to keep cores at low power status for sufficient period of time [8]. However the lack of the solid EM transient models hinders the development of optimization techniques for such kind of effects.

In this article, we propose new physics-based dynamic EM model and assessment technique to deal with the stress recovery effect in interconnect wires stressed by the arbitrary (unipolar or bipolar) time-varying current waveforms and varying temperature. Such dynamic EM model is in contrast to the existing EM models, which assume that the wire is stressed under constant current density and temperature. The new model is developed by the analytical solution of the one-dimensional Korhonen's equation with the time-varying electric current and temperature loads [9]. The model can explain many of the experimentally observed transient stress recovery effects caused by various current waveform patterns [5–7]. More significantly, the new EM model open the new opportunities to manage EM reliability at the circuit, system, and even server/rack/data center levels without additional design costs. A comparison of the predicted analytic stress evolution kinetics with the results generated by the direct numerical calculation of the continuity equation with the finite element analysis (FEA) tool has demonstrated an excellent agreement.

The article is organized as follows: Section 2 reviews the physics and existing models of electromigration. Section 3 introduces the new dynamic EM model considering the time-varying current density and temperature. The EM stress recovery effect and the limitation of using the effective DC for failure prediction and EM immortal check are discussed in Section 4. Section 5 presents the formalism describing the evolution of the metal line resistance caused by void volume evolution under different time-dependent current density and temperature stressing. Section 6 presents the potential of the application of the proposed EM model for reliability-aware energy-efficient computing at system level. Section 7 concludes the article.

2. Background and review of existing works

2.1. Existing modeling based on effective direct current

Existing EM models such as the semi-empirical Black's equation, which is widely used in industry, are based on the DC load of a single confined metal wire keeping at the constant temperature [10]. In order to consider the stress buildup caused by the transient current waveforms in a typical VLSI chip, which can be unipolar, such as in the power grid networks, or bipolar, such as in the signal nets, the time-dependent current density waveforms are converted to the so-called EM effective DC current:

$$j_{\mathrm{trans,EM,eff}} = \frac{1}{P}\left(\int_0^P j_+(t)dt - \gamma\int_0^P |j_-(t)|dt\right) \quad (1)$$

where $j_+(t)$ and $j_-(t)$ are the current densities of the positive and negative phases of the bipolar current, γ is the EM recovery factor, P is the period of the current waveform. When the current density is unidirectional, $j_{\mathrm{trans,EM,eff}}$ is the time averaged current density. However, using the effective current formula in Eq. (1) will create several problems [6]. First, the recovery factor depends on the specific current waveforms and is not constant. Second, it ignores important transient effects. For instance, we may have the driving current waveform, which makes the peak stress exceed the critical stress while the average current never leads to void nucleation (wire is immortal).

To mitigate this problem, a number of *dynamic* EM models, which consider the time-dependent current waveforms, have been proposed [11–13]. However, the EM model in [13] is still based on traditional semi-empirical Black's equation, where the current density exponent is not a constant but a function of residual stress and current density. Especially, the recovery effect is not properly considered and the weighted average current is still used. Recently, a new dynamic EM model was proposed [14]. However, this model is based on Korhonen's continuity equation with constant current density. It fails to predict stress recovery effect as we show in this work and inappropriately predicts increasing/constant stress when current changes are significant: reducing to a much smaller value or turning off.

2.2. EM physics and governing equations

EM is a physical phenomenon caused by current-induced atom diffusion in the direction of the electron flow due to momentum exchange between lattice atoms and charge carriers. This oriented atomic flow results in metal density depletion and accumulation at the ends of the wire, where the atomic migration is blocked by diffusion barriers. When the hydrostatic stress develops, the stress gradient along the wire would lead to the drift of lattice atoms in the direction opposite to the direction of the electric current.

As shown in Fig. 2, the steady state will be reached when the backward flux compensates the current-induced flux, and the stress will be linearly distributed along the wire. Fig. 2(a) shows the stress evolution along the wire (with the left end as the cathode node and right as the anode node). This is a typical hydrostatic stress evolution pattern driven by DC current. But if the driving current is time-varying, the stress might not be monotonically increasing with time. For instance, if the current density is reduced at some instance in time, then the current induced flux can be smaller than the stress gradient induced atomic backflow, and the atom migration direction can even be reversed leading to a reduction of the hydrostatic stress as shown in Fig. 1. Such transient recovery can make the stress evolution take longer time to reach the critical stress for void nucleation. As a result, it can help extend the lifetime of the wires.

Fig. 2(b) shows the evolution of the electric current induced hydrostatic stress at the cathode end of a metal wire (biggest tensile stress) under different DC densities and temperatures. It indicates that

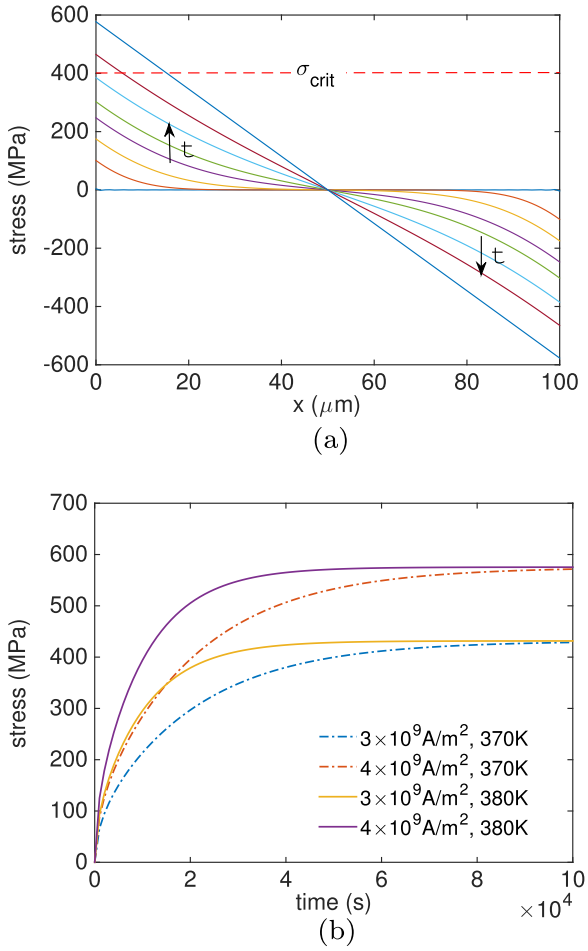

Fig. 2. Evolution of hydrostatic stress (a) along the wire and (b) at the cathode end over time stressed under different current densities and temperatures, in the case of zero initial stress.

both the current density and the temperature affect the stress evolution rate. For a one-dimensional metal line confined by diffusion barriers, the stress evolution is described by the well-known Korhonen's equation [15]:

$$\frac{\partial \sigma}{\partial t} = \frac{\partial}{\partial x}\left[\kappa\left(\frac{\partial \sigma}{\partial x} + \frac{eZ\rho j}{\Omega}\right)\right] \tag{2}$$

Here, $\kappa = DB\Omega/k_BT$ where $D = D_0 \exp(-Ea/k_BT)$ is the atomic diffusivity which depends on temperature, B is the bulk modulus, Ω is the atomic volume, E_a is the activation energy, k_B is Boltzmann's constant, and eZ is the effective charges of the migrating atoms. In Eq. (2) current density and temperature are assumed to be uniformly distributed along the line. Solution of this initial-boundary value problem for a finite wire with two blocked ends locates at x=0 and l is the infinite series:

$$\sigma = \sigma_T + \frac{eZ\rho jl}{\Omega} \times \left[\frac{1}{2} - \frac{x}{l} - 4\sum_{n=0}^{\infty} \frac{\cos(\frac{(2n+1)\pi x}{l})}{(2n+1)^2\pi^2} e^{-\frac{(2n+1)^2\pi^2}{l^2}\kappa t}\right] \tag{3}$$

Here, l is the wire length, j is the current density, σ_T is the thermal stress developed in the metal wire confined in the inter-layer dielectric/inter-metal dielectric (ILD/IMD) during cooling from the zero stress temperature down to the temperature of use condition. Approximate value of void nucleation time (t_{nuc}) can be extracted from this solution, as an instant in time when stress at the cathode end of the wire (x=0) reaches σ_{crit} [16,17].

Table 1
Parameters and typical values.

Parameter	Value	Parameter	Value
E_a	0.86 eV	B	1×10^{11} Pa
Z	10	Ω	1.66×10^{-29} m^3
σ_{crit}	400 MPa	ρ	3×10^{-8} Ω
l	1×10^{-4} m	D_0	7.56×10^{-5} m^2/s

3. New model for the EM-induced stress evolution caused by time-dependent current density and temperature

In this section, we present the new dynamic EM model considering the time-varying current density and temperature. This model was originally derived from the analytical solution of the continuity equation (2) for a metal wire loaded by the time-varying electric current. We further extended the model to take into account the time-varying temperature. The resulting model can analyze the stress evolution kinetics caused by any time-varying currents and temperatures.

To validate the proposed model, detailed numerical simulation of the continuity equation (2) should be employed. In this work, we do numerical simulation using the FEA tool COMSOL [18]. Before we proceed, we list values of all employed parameter in Table 1. Also, to simplify our numerical analysis, we keep the thermal (residual) stress (σ_T) equals zero.

3.1. Generalized EM-induced stress evolution model with the arbitrary piecewise constant current

In this subsection, we first present the governing stress evolution equation with time-varying current waveforms. The stress evolution takes place in an initially void-less interconnect line. To simplify the analysis, we first assume that only the current density changes over time, i.e. the temperature is constant. Later on, we extend the derived stress evolution expression to consider time-varying temperature.

3.1.1. Dynamic EM model considering arbitrary time-varying currents

In the case of time-dependent current density, one-dimensional continuity equation (2) can be converted into the following nonhomogeneous form [9]:

$$\frac{\partial(\sigma + \frac{eZ\rho j}{\Omega}(x - \frac{l}{2}) - \sigma_T)}{\partial t} - \kappa\frac{\partial^2}{\partial x^2}\left(\sigma + \frac{eZ\rho j}{\Omega}\left(x - \frac{l}{2}\right) - \sigma_T\right) = \frac{eZ\rho j}{\Omega}\left(x - \frac{l}{2}\right)\frac{\partial j}{\partial t} \tag{4}$$

with the boundary condition: $\frac{\partial \sigma}{\partial t}|_{x=0,l} = -\frac{eZ\rho j}{\Omega}$ and the initial condition: $\sigma(x, t = 0) = \sigma_T$. As it was shown in [9], Eq. (4) can be solved analytically. The analytical solution for stress evolution kinetics takes the form:

$$\sigma(x, t) = \sigma_T + \frac{4eZ\rho}{\Omega l}\kappa\sum_{n=0}^{\infty}\cos\frac{(2n+1)\pi x}{l} e^{-\frac{(2n+1)^2\pi^2}{l^2}\kappa t} \times \int_0^t j(t) e^{\frac{(2n+1)^2\pi^2}{l^2}\kappa\tau} d\tau \tag{5}$$

Solution Eq. (5) is valid for any arbitrary time-varying current waveform $j(t)$. It is not difficult to show that Eq. (5) converts to the standard stress evolution kinetics equation (3) if the current density is constant (DC current).

In practical application, the current or power inputs of a chip are better modeled as time-varying piece-wise constant as the chip may be in different stable performance/power states for a period of time

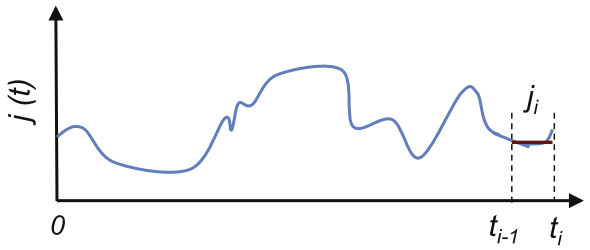

Fig. 3. A random time-dependent current density waveform where piecewise constant method can be applied.

instead of changing all the time. In this work, we divide a given time period [0, t] into i intervals and in each interval Δt_i, we have constant temperature and current density. The time interval can be decided based on the computational complexity and precision requirement. A large interval is chosen at low frequency. Assume that we have computed the stress at t_{i-1} and want to predict the stress at $t_i = t_{i-1} + \Delta t_i$ as shown in Fig. 3. Then we have the following iterative stress computation formula:

$$\sigma(x, t_i) = \sigma_T + \frac{4eZ\rho}{\Omega l}\sum_{n=0}^{\infty}\cos\frac{(2n+1)\pi x}{l}\phi(t_i) \tag{6}$$

where

$$\phi(t_i) = e^{-\frac{(2n+1)^2\pi^2}{l^2}\kappa\Delta t_i}\left[\kappa\int_0^{\Delta t_i} j_i e^{\frac{(2n+1)^2\pi^2}{l^2}\kappa\tau}d\tau + \phi(t_{i-1})\right] \tag{7}$$

and

$$\phi(t_1) = e^{-\frac{(2n+1)^2\pi^2}{l^2}\kappa\Delta t_1}\kappa\int_0^{\Delta t_1} j_1 e^{\frac{(2n+1)^2\pi^2}{l^2}\kappa\tau}d\tau \tag{8}$$

Here, j_i is the constant current density value during the time interval $[t_{i-1}, t_i]$. Note that $\frac{4eZ\rho}{\Omega l}\sum_0^{\infty}\cos\frac{(2n+1)\pi x}{l}\phi(t_{i-1})$ presents EM stress at t_{i-1}, which is caused by the driving current $j(t)$ from the very beginning (t=0) to the time instant $t = t_{i-1}$. So the accumulated hydrostatic stress at the instant in time $t = t_i$ can be easily calculated based on Eq. (6) if $\phi(t_{i-1})$ is provided. Fig. 4 shows an example of the stress evolution at the cathode end of the metal wire under time-varying current and constant temperature loads. The solution obtained from Eq. (6) agrees well with the result of numerical solution of Eq. (2).

3.1.2. Dynamic EM model considering both time-varying current and temperature

Temperature affects atomic diffusivity and is reported to have huge (exponential) impacts on the lifetime of the wire due to EM effects [19,17]. The on-chip temperature changes along with the change of chip workloads (power dissipation). Thus it is necessary to

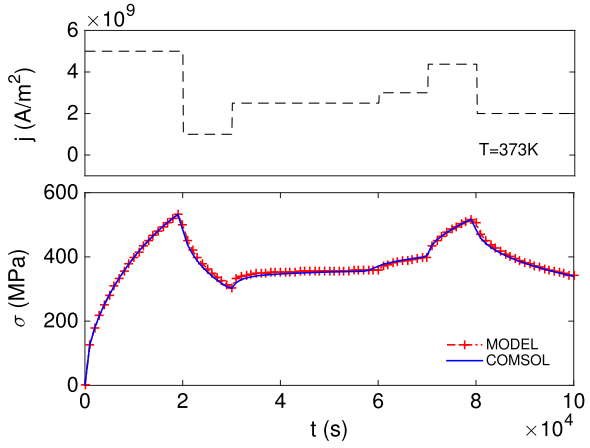

Fig. 4. Stress evolution under time-varying current load with constant temperature.

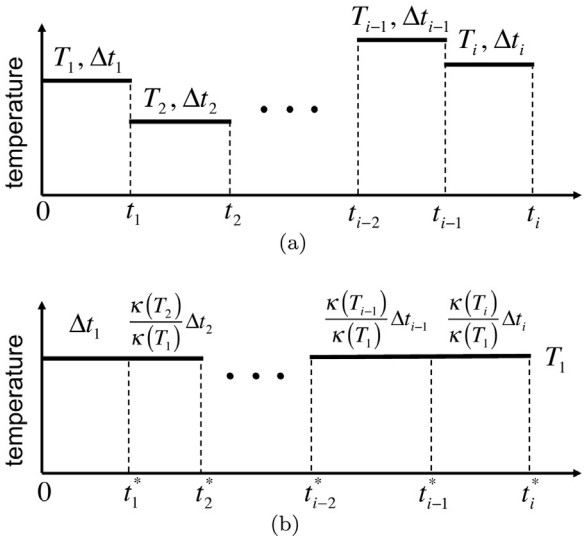

Fig. 5. (a) Original time-dependent temperature waveform and (b) constant temperature with equivalent time intervals.

consider the effect of time-varying temperature in EM modeling. In this work, we employ the equivalent time scheme to account for the dynamic temperature effect, which uses expressions for stress build-up under constant temperature to describe the stress evolution under time-varying conditions [13,14].$\kappa(T(t))$ is the term that is affected by temperature:

$$\kappa(T(t)) = \frac{D_0\exp(-Ea/k_BT(t))B\Omega}{k_BT(t)} \tag{9}$$

It has been observed that, if the atomic diffusivity is assumed to be independent of the stress, the temperature impact on the stress $\sigma(T, t)$ through $\kappa(T(t))$ can be translated to the time period change for a metal wire. In other words, as demonstrated in Fig. 5, the stress developed on the wire over time interval Δt_i under temperature T_i is equal to the stress developed over time interval $\frac{\kappa(T_i)}{\kappa(T_1)}\Delta t_i$ under temperature T_1. As a result, the problem of analyzing stress evolution considering both time-varying current density and temperature becomes estimating stress evolution under dynamic current stress while temperature is constant ($T = T_1$), which has been discussed in Section 3.1.1. Thus we replace the time intervals Δt_i in Eqs. (7) and (8) with new time intervals $\Delta t_i^* = \frac{\kappa(T_i)}{\kappa(T_1)}\Delta t_i$ and apply constant temperature $T = T_1$. The stress at t_i considering time-varying current density and temperature can be calculated as:

$$\sigma(x, t_i) = \sigma_T + \frac{4eZ\rho}{\Omega l}\sum_{n=0}^{\infty}\cos\frac{(2n+1)\pi x}{l}\phi(t_i) \tag{10}$$

where

$$\begin{aligned}\phi(t_i) &= e^{-\frac{(2n+1)^2\pi^2}{l^2}\kappa(T_1)\frac{\kappa(T_i)}{\kappa(T_1)}\Delta t_i}\times\left[\kappa(T_1)\int_0^{\frac{\kappa(T_i)}{\kappa(T_1)}\Delta t_i} j_i e^{\frac{(2n+1)^2\pi^2}{l^2}\kappa(T_1)\tau}d\tau + \phi(t_{i-1})\right]\\ &= e^{-\frac{(2n+1)^2\pi^2}{l^2}\kappa(T_i)\Delta t_i}\times\left[\kappa(T_1)\int_0^{\Delta t_i} j_i e^{\frac{(2n+1)^2\pi^2}{l^2}\kappa(T_1)\frac{\kappa(T_i)}{\kappa(T_1)}\tau}\frac{\kappa(T_i)}{\kappa(T_1)}d\tau + \phi(t_{i-1})\right] = e^{-\frac{(2n+1)^2\pi^2}{l^2}\kappa(T_i)\Delta t_i}\times\left[\kappa(T_1)\int_0^{\Delta t_i} j_i e^{\frac{(2n+1)^2\pi^2}{l^2}\kappa(T_i)\tau}d\tau + \phi(t_{i-1})\right]\end{aligned} \tag{11}$$

and

$$\phi(t_1) = e^{-\frac{(2n+1)^2\pi^2}{l^2}\kappa(T_1)\Delta t_1}\kappa(T_1)\int_0^{\Delta t_1} j_1 e^{\frac{(2n+1)^2\pi^2}{l^2}\kappa(T_1)\tau}d\tau \tag{12}$$

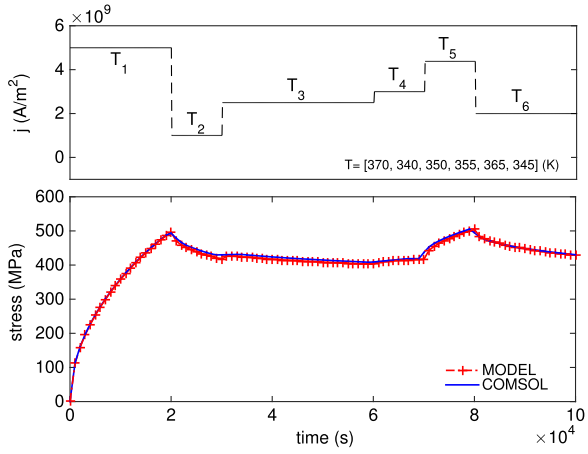

Fig. 6. Stress evolution under time-varying current and temperature stressing.

Now we are able to predict the EM-induced stress evolution under time-varying current load with time-varying temperature based on Eq. (10). Fig. 6 shows an example of the stress evolution at the cathode end of the metal wire caused by dynamic current load, which refers for instance, to a core working in different power states. Since the time scale for each state is much longer than thermal time constant, we assume that each state corresponds to a constant temperature value. We have compared the obtained analytical solution with the result of numerical solution of Eq. (2) with the known $j(t)$ and $T(t)$ and have obtained an excellent agreement as shown in Fig. 6.

It can be observed from Eq. (11) that, different from the expressions in [13,14] which need to translate the actual time intervals Δt_i to the equivalent time intervals $\frac{\kappa(T_i)}{\kappa(T_1)}\Delta t_i$ during the stress computation, the final expression of our proposed stress evolution model includes only the actual time-interval Δt_i and the actual temperature T_i during the time interval Δt_i. Besides, Eq. (11) differs from Eq. (7) only in that it uses a time-dependent temperature T_i instead of a constant temperature. Thus the proposed model naturally considers the temperature change. It also should be noted that the derived general discretization formula equation (10) can be applied to any time-varying current densities and temperature waveforms, and at the same time correctly predicts stress recovery effect, which is ignored in all existing ad hoc methods [13,14].

3.2. EM modeling for periodic pulse current

Another interesting case is the driving currents are periodic pulse waveforms, which can be found in the typical clock networks and in some signal networks as well. In this case, the computation of the stress evolution can be simplified. Let us consider, for instance, the current density profiles shown in Fig. 7, which are good approximations for real power traces in the practical situations. Specifically, we assume that the current density $j(t)$ has the following form:

$$j(t) = \begin{cases} j_1, & mP \le t < mP + t_1, \\ j_2, & mP + t_1 \le t < (m+1)P, \end{cases} \tag{13}$$

We note that j_1 and j_2 can be in the same phase or in opposite phases of the pulse, P is the period of the current waveform. For large time scales, which is longer than thermal time constant, we can assume that the temperature profile has similar form:

$$T(t) = \begin{cases} T_1, & mP \le t < mP + t_1, \\ T_2, & mP + t_1 \le t < (m+1)P, \end{cases} \tag{14}$$

In this case, the stress evolution expression considering periodic pulsed current waveform can be derived based on Eq. (10):

- **If** $mP \le t < mP + t_1$ $(\tau = t - mP)$:

$$\sigma(x,t) = \sigma_T + \frac{4eZ\rho}{\Omega l}\sum_{n=0}^{\infty}\cos\frac{(2n+1)\pi x}{l}e^{-\frac{(2n+1)^2\pi^2}{l^2}\kappa_1\tau} \times\left(\kappa_1\int_0^{\tau} j_1 e^{\frac{(2n+1)^2\pi^2}{l^2}\kappa_1\tilde{\tau}}d\tilde{\tau} + M\phi_P\right) \tag{15}$$

where

$$\phi_P = e^{-\frac{(2n+1)^2\pi^2}{l^2}(\kappa_1 t_1+\kappa_2 t_2)}\kappa_1\int_0^{t_1} j_1 e^{\frac{(2n+1)^2\pi^2}{l^2}\kappa_1\tilde{\tau}}d\tilde{\tau} + e^{-\frac{(2n+1)^2\pi^2}{l^2}\kappa_2 t_2}\kappa_2\int_0^{t_2} j_2 e^{\frac{(2n+1)^2\pi^2}{l^2}\kappa_2\tilde{\tau}}d\tilde{\tau} \tag{16}$$

- **If** $mP + t_1 \le t < (m+1)P$ $(\tau = t - mP - t_1)$:

$$\sigma(x,t) = \sigma_T + \frac{4eZ\rho}{\Omega l}\sum_{n=0}^{\infty}\cos\frac{(2n+1)\pi x}{l}e^{-\frac{(2n+1)^2\pi^2}{l^2}\kappa_2\tau} \times\left(\kappa_2\int_0^{\tau} j_2 e^{\frac{(2n+1)^2\pi^2}{l^2}\kappa_2\tilde{\tau}}d\tilde{\tau} + \phi_1 + M\phi_P\right) \tag{17}$$

where

$$\phi_1 = e^{-\frac{(2n+1)^2\pi^2}{l^2}\kappa_1 t_1}\kappa_1\int_0^{t_1} j_1 e^{\frac{(2n+1)^2\pi^2}{l^2}\kappa_1\tilde{\tau}}d\tilde{\tau} \tag{18}$$

$$\phi_P = e^{-\frac{(2n+1)^2\pi^2}{l^2}(\kappa_1 t_1+\kappa_2 t_2)}\left(\phi_1 + \kappa_2\int_0^{t_2} j_2 e^{\frac{(2n+1)^2\pi^2}{l^2}\kappa_2\tilde{\tau}}d\tilde{\tau}\right) \tag{19}$$

In both cases, we have

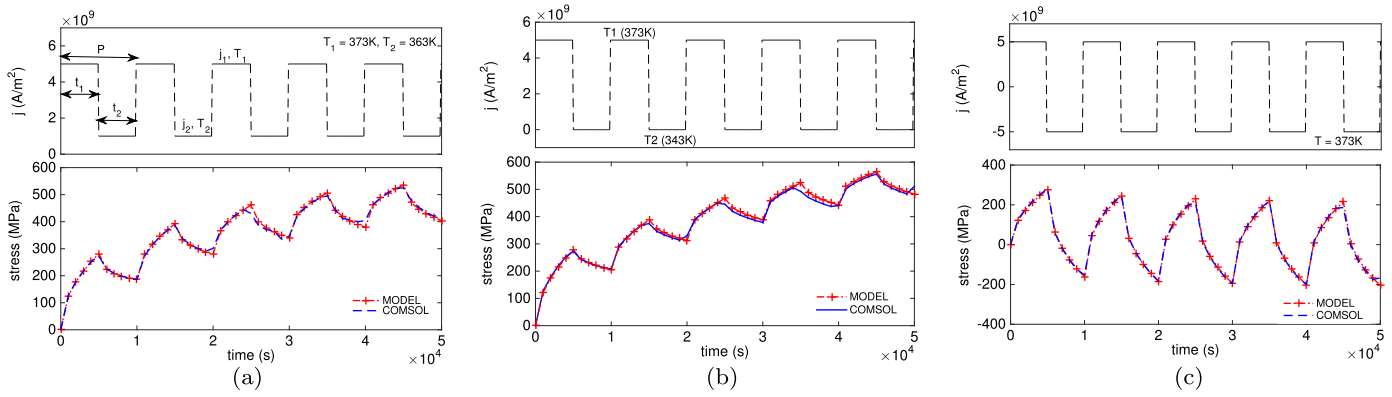

Fig. 7. Stress evolution caused by periodic (a), (b) unipolar and (c) symmetrical bipolar pulse current densities at cathode end of the metal line.

$$t_2 = P - t_1 \quad M = \frac{1 - e^{\frac{-(2n+1)^2\pi^2}{l^2}m(\kappa_1 t_1 + \kappa_2 t_2)}}{1 - e^{\frac{-(2n+1)^2\pi^2}{l^2}(\kappa_1 t_1 + \kappa_2 t_2)}}\kappa_1 = \frac{D_0 e^{-\frac{E_a}{k_B T_1}} B\Omega}{k_B T_1} \quad \kappa_2 = \frac{D_0 e^{-\frac{E_a}{k_B T_2}} B\Omega}{k_B T_2}$$

The proposed model for periodic pulse current has been validated by results of numerical simulations as shown in Fig. 7. Figs. 7(a) and (b) correspond to unipolar pulsed current density waveforms, where the former one has two nonzero magnitudes, while Fig. 7(c) is the case of symmetrical bipolar pulsed current density. Significant stress variation caused by dynamical current loads is observed. We will discuss this phenomenon in the next section.

4. Study of the EM stress recovery

EM process is composed of the void nucleation phase followed by the void growth. As it was mentioned above, the void is generated from the preexisting flaw existing in the metal when the EM-induced hydrostatic tensile stress exceeds the critical one. In this section, we focused on the analysis of EM stress recovery process in the first phase where the void has not been nucleated. The recovery effect of hydrostatic stress described in this section is based on the proposed new dynamic EM model.

4.1. EM stress recovery effect

As shown in the previous sections, EM recovery happens when the current density goes down temporarily. In Fig. 7, the hydrostatic stress is reduced when the current density jumps from j_1 to a much smaller value j_2. As a result, it takes longer time for the stress to reach the critical value, thus results in a longer lifetime. The EM recovery effect is mainly caused by the net atomic backflow, which relaxes the stress. This phenomenon can be easily understood when atoms change their migration direction in the opposing phase of bipolar stressing. On the other hand, even when j_1 and j_2 are in the same direction, it is still possible that the net atom flow can change their direction. The reason is that when current is decreasing, the atomic backward flux caused by an accumulated stress gradient will prevail the electronic current induced flux and we will have a temporal reduction in the stress. Fig. 8 shows the analysis of the stress recovery for a single pulse current case. Fig. 8(a) refers to the schematics for current density and temperature.

To further study the recovery effects, we first fix the temperature and investigate EM recovery under different magnitudes of current density change as shown in Fig. 8(b). Then we investigate the impact of temperature on stress evolution considering different current loads. Fig. 8(c) describes the stress recovery when current is switched off, while Fig. 8(d) corresponds to constant current stressing. The observations are summarized as follows:

- There could be no stress recovery when current density difference is small, for example the $j_2/j_1 = 0.95$ curve in Fig. 8(b). This is because the electron flow induced forward flux can be still larger than the stress gradient induced backward flux when current density reduces from j_1 to j_2. Thus the atoms keep diffusing from the cathode end to the anode end along the metal line, results in continuous accumulation of the stress. The backward atomic flux caused by stress gradient could be larger than the current induced forward flux if the current density difference is significant, where an extreme case is the current switched off at an instant in time $t = t^*$. This atomic backflow will be gradually reducing over time and finally the system will reach a new equilibrium state corresponding to the new current density.
- As shown in Fig. 8(c), the accumulated stress starts to relax when current is turned off. This process is described by an exponential decay with the time constants $\tau_0^{(2n+1)} = l^2/\kappa\pi^2(2n+1)^2 = \tau_0/(2n+1)^2$, determined by the atomic diffusivity. We observe that higher temperature can speed up atom diffusion towards the cathode end and lead to more recovery. This is contrary to the non-recovery case, for instance the metal wire stressed by constant current as demonstrated in Fig. 8(d), where higher temperature results in faster stress accumulation than a shorter lifetime.

4.2. Limitation of using effective DC methods

For unidirectional current, the time-averaged or other weighted averaged currents have been used as the effective DC in existing EM analysis. However, we show in this subsection that using the effective DC for failure predication and immortal wire detection can lead sometime to wrong results.

It is well known that the Blech rule has been employed for the out filtration of immortal wire segments with diffusion blocking boundaries [20]. The interconnect will not fail if the product of $(j \times l)$ is smaller than the critical value, defined as:

$$(j \times l)_{crit} = \frac{2\Omega\sigma_{crit}}{eZ\rho} \tag{20}$$

Now let us look at one particular case. Assuming at a constant temperature, we set the average current density (j_{avg}) to 2.5×10^9 A/m^2 so that $(j_{avg} \times l) < (j \times l)_{crit}$, which means that the metal line is EM immortal under the average current model using the Blech rule. However, based on the proposed dynamic model, which is also the actual numerical analysis results as shown in Fig. 9(a), we find that stress can go above the critical stress σ_{crit}, indicating that the void will be nucleated in this case. Note that the kinetics of stress evolution is caused by unipolar pulse current of 30% duty cycle in Fig. 9(a).

Fig. 9(b) further shows the lifetimes of a wire caused by UPC under different duty cycles (duty cycle=1 means DC current) with the same average current density using the proposed EM model. We also show the lifetime of a wire caused by the peak current of the UPC. From the figure, we can observe that the wire would fail by UPC stressing when duty cycle $\leq$40% (when the curve starts to appear in the figure). However, if we use the average current density for the calculation, as shown in the previous figure, the wire will never fail by EM. So the effective DC method can lead to optimistic EM estimation, which can be dangerous for practical EM sign-off. On the other hand, simply applying worst-case current density would lead to too conservative results, limiting the design space for reliability-performance trade-off. Traditionally, the EM failure for a single confined metal line is considered as, for example, 10% line resistance increase. So far, we have discussed a phenomenon of the void nucleation, which by itself cannot increase the line resistance. Void growth following its nucleation is responsible for this increase. As it was shown in [17], it is pretty straightforward to account the void volume growth for the accurate estimation of the line lifetime. But, taking into consideration the noticeable redundancy existing in on-chip interconnects, we can conclude that the failure of an individual line of the power/ground grids cannot result in the interconnect failure. New criterion for the EM-induced chip failure was proposed in a number of works, see for example [21,17]. To be more specific, EM-induced voltage drop degradation above the spec should be considered as the failure criteria for the full-chip EM assessment [17].

All the above results were obtained for the low frequency currents with time intervals comparable to time constant τ_0, which is close to minutes or hours. Time-varying current or power profiles in those cases are more likely to be caused by power/energy management at server/rack/data center levels, where the currents under analysis are mainly carried by the power/ground nets. However, the chip level power

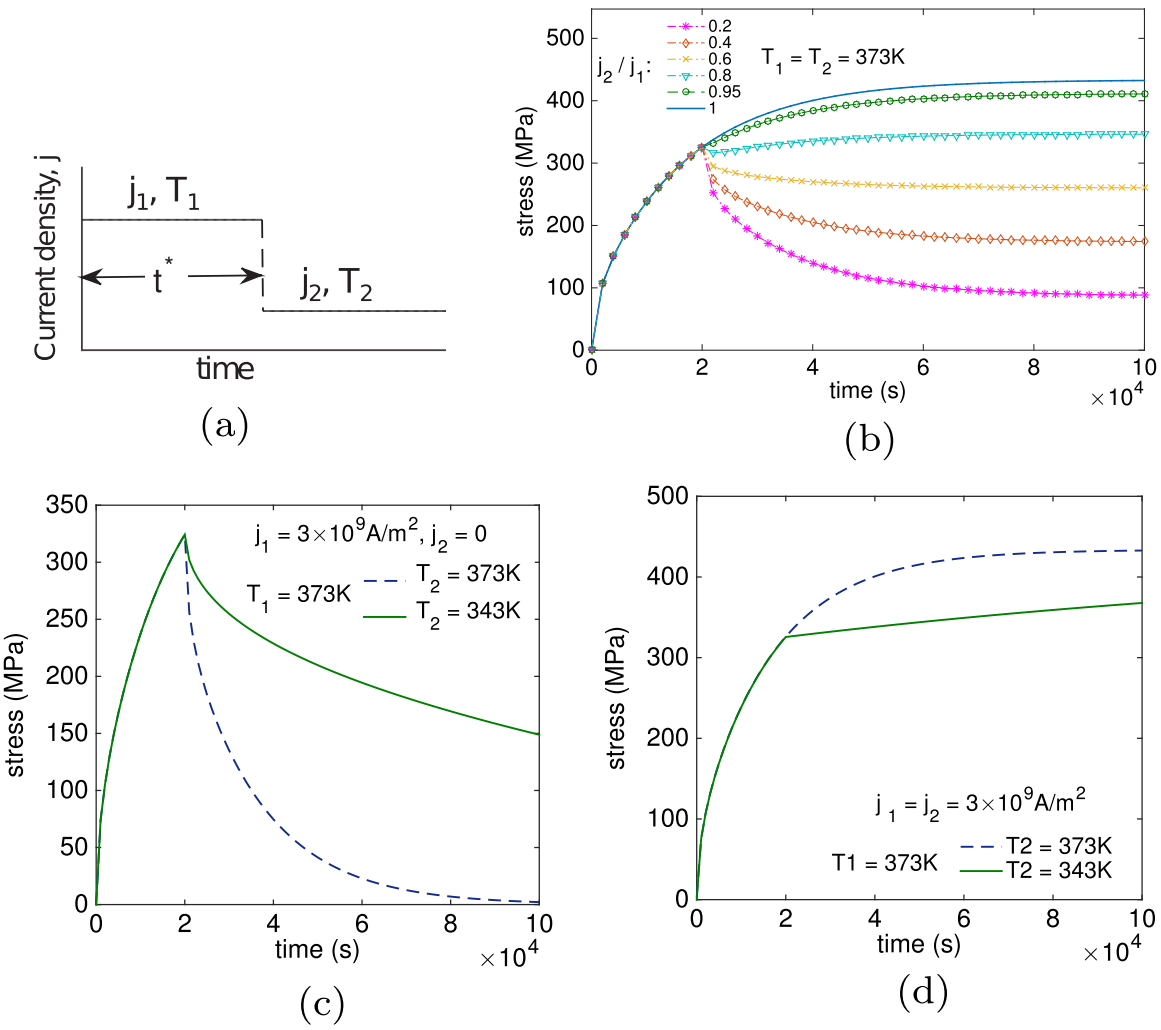

Fig. 8. (a) Time dependent current density and temperature waveform, (b) EM recovery considering different current density change magnitudes at constant temperature, (c) stress relaxation when current is switched off at different temperatures, and (d) stress evolution caused by DC current at different temperatures.

management and scheduling may operate at millisecond level and chip clocks may operate in the MHz and GHz ranges. Fig. 10 analyzes the stress evolution in a metal line caused by UPC and symmetrical BPC at 1 MHz frequency, which corresponds to the signal lines in the circuit. We can observe from the figure that, at high frequencies, the averaged DC currents can be good estimations of the unipolar and bipolar pulsed currents.

In this case, the time-dependent current induced stress fluctuates (~0.01 MPa) around the curve, which describes the stress evolution generated by the effective DC current. This is because at high frequencies, the time intervals are much shorter than τ_0 so that the system cannot reach a new equilibrium state corresponding to the new applied current by means of atom diffusion. In Fig. 10(b), stress fluctuates around zero for symmetrical bipolar pulse current. It indicates complete EM recovery during current reversal, and has been experimentally observed in [7]. Thus high frequency symmetrical bipolar current will not cause EM failure in interconnects. As discussed in [22,9], thermal cycling induced thermal fatigue and cracks caused by diffusive mechanism and interface properties may be a cause. Those failure mechanisms can also explain the failures observed by symmetrical bipolar pulse current stressing in [11,6].

5. Kinetics of resistance degradation in metal line

In this section, we consider the void growth phase and develop the formalism that describes the evolution of the metal line resistance caused by current induced evolution of the void volume. To emphasize the current induced void size change, the residual stresses such as σ_T are ignored in the analysis.

5.1. Resistance degradation caused by DC current at constant temperature

A metal line embedded in the rigid confinement and cooled from the zero stress temperature down to the test temperature can have void nucleated caused by the generated thermal stress when the stress is larger than a critical value. In this case, the void volume is determined by the relaxation of the preexisted tensile strain, and by zero stress everywhere else in the metal. The void locating at the end of the line starts changing its volume when an electrical stressing is applied to this line. In the case of DC stressing, a void located at the cathode end of line will be growing by means of migration of the void surface atoms to the metal bulk. Once the stress field evolution is solved, the void volume kinetics $V(t)$ is calculated from the volume of atoms drifted into the line:

$$V(t) = -WH \int_0^L \frac{\sigma(x, t)}{B} \tag{21}$$

Here W and H are the line width and thickness schematically shown in Fig. 11. The evolution of void volume under DC current stressing and constant temperature has the form:

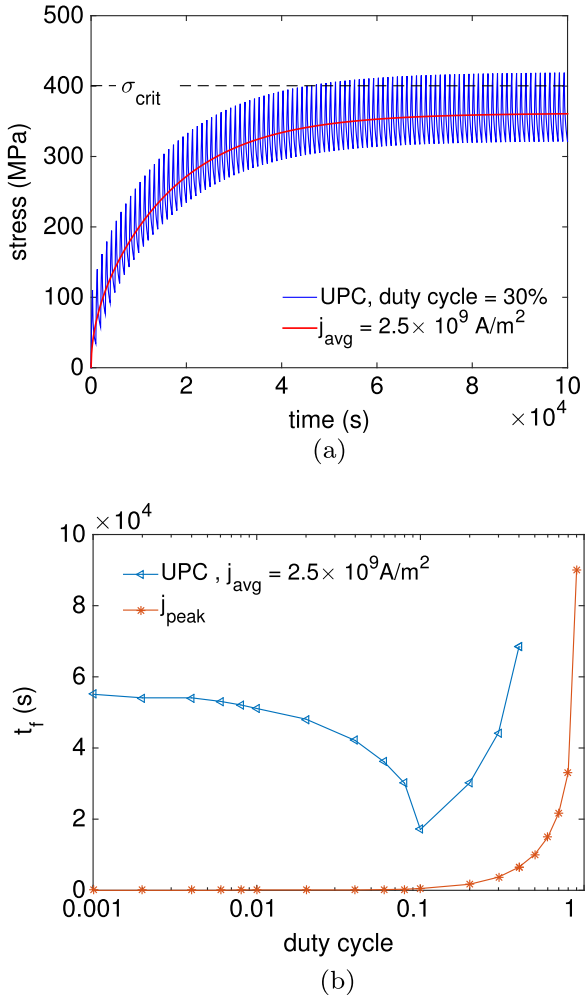

Fig. 9. (a) Stress evolution at the cathode end of the metal line caused by the unipolar pulse current (UPC) with duty cycle=30% and averaged DC current, (b) EM lifetimes for UPC load with various duty cycles compared with lifetimes caused by constant peak current load. Here, j_{avg} is fixed to 2.5×10^9 A/m^2 so that $(j_{avg} \times l) < (j \times l)$, T=373 K.

$$V(t) = WH\frac{eZ\rho jl^2}{2\Omega B}\left[1 - \frac{32}{\pi^3}\sum_{n=0}^{\infty}\frac{(-1)^n}{(2n+1)^3}e^{-\kappa\frac{(2n+1)^2\pi^2}{4l^2}t}\right] \tag{22}$$

Assuming that the void occupies the whole cross section of the line and the current is forced to flow through the barrier layer at that portion of the line, the change of the line resistance caused by the growing void can be calculated as:

$$\Delta R(t) = \frac{V(t)}{WH}\left[\frac{\rho_{\mathrm{Ta}}}{h_{\mathrm{Ta}}(W+2H)} - \frac{\rho_{\mathrm{Cu}}}{WH}\right] \tag{23}$$

where ρ_{Ta} and ρ_{Cu} are the resistivities of the barrier material (Ta/TaN) and copper, h_{Ta} is the barrier layer thickness. Thus, in the case of DC stressing, the kinetics of line resistance change is described as:

$$\Delta R(t) = \frac{eZ\rho jl^2}{2\Omega B}\left[\frac{\rho_{\mathrm{Ta}}}{h_{\mathrm{Ta}}(W+2H)} - \frac{\rho_{\mathrm{Cu}}}{WH}\right] \times\left[1 - \frac{32}{\pi^3}\sum_{n=0}^{\infty}\frac{(-1)^n}{(2n+1)^3}e^{-\kappa\frac{(2n+1)^2\pi^2}{4l^2}t}\right] \tag{24}$$

Fig. 12 shows an example of the kinetics of line resistance degradation under current density $j = 5 \times 10^9$ A/m^2 at $T = 373$ K. We use $l = 1$ μm, $H = 120$ nm, $W = 200$ nm and $h_{\mathrm{Ta}} = 10$ nm in the simulation.

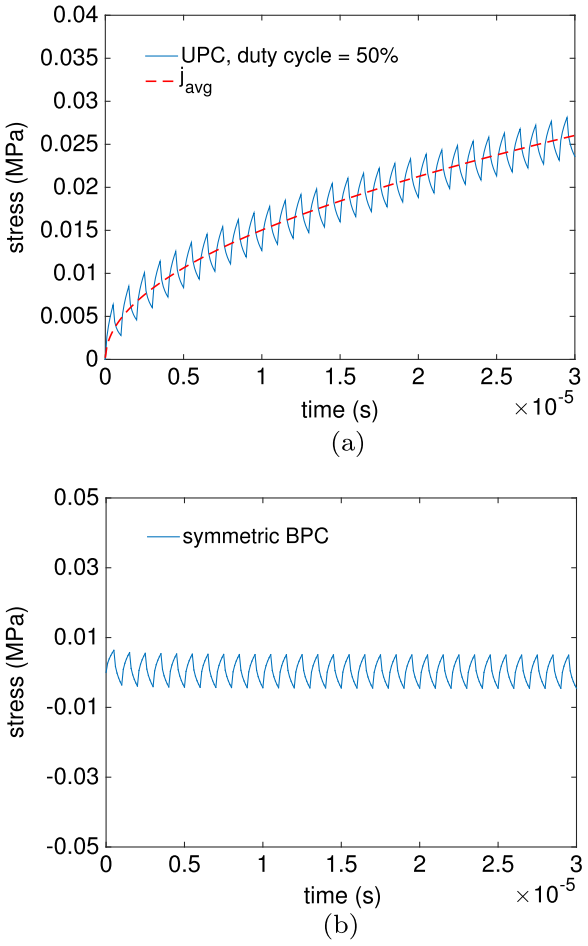

Fig. 10. Stress evolution at the cathode end of the metal line caused by unipolar pulse (UPC) with duty cycle=50% and symmetrical bipolar pulse current (BPC) loads at T=400 K.

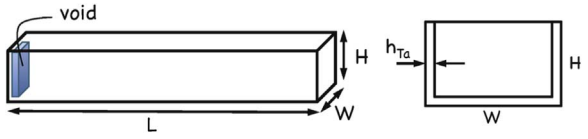

Fig. 11. Schematics of the line geometry.

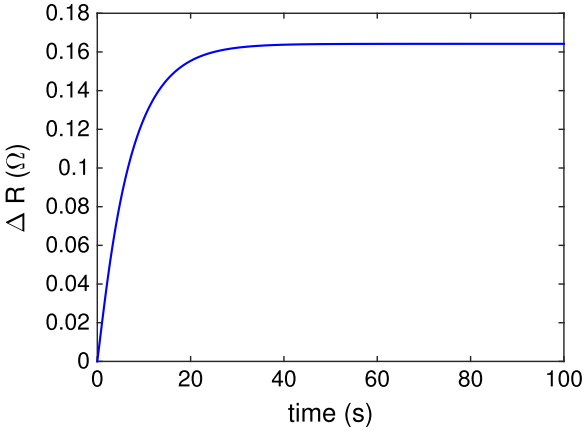

Fig. 12. Kinetics of line resistance change caused by constant current stressing under constant temperature.

5.2. Resistance degradation caused by time-dependent current density and temperature

Similarly, when time-dependent current densities and temperatures are loaded to the line with the preexisted void, we can calculate the void volume evolution and the kinetics of resistance change according to stress evolution obtained from (4). For arbitrary piecewise constant currents and temperatures, the void volume at instance in time $t = t_i$ can be expressed as:

$$V(t_i) = -WH\frac{4eZ\rho}{\Omega B}\sum_{n=1}^{\infty}\frac{(-1)^n}{2n-1}\psi(t_i) \tag{25}$$

where

$$\psi(t_i) = e^{-\frac{(2n-1)^2\pi^2}{4l^2}\kappa(T_i)\Delta t_i}\times\left[\kappa(T_i)\int_0^{\Delta t_i} j_i e^{\frac{(2n-1)^2\pi^2}{4l^2}\kappa(T_i)\tau d\tau} + \psi(t_{i-1})\right] \tag{26}$$

and

$$\psi(t_1) = e^{-\frac{(2n-1)^2\pi^2}{4l^2}\kappa(T_1)\Delta t_1}\kappa(T_1)\int_0^{\Delta t_1} j_1 e^{\frac{(2n-1)^2\pi^2}{4l^2}\kappa(T_1)\tau d\tau} \tag{27}$$

Here $\Delta t_i = t_i - t_{i-1}$. The corresponding resistance change at $t = t_i$ can be described as:

$$R(t_i) = -\frac{4eZ\rho}{\Omega B}\left[\frac{\rho_{Ta}}{h_{Ta}(W+2H)} - \frac{\rho_{Cu}}{WH}\right]\times\sum_{n=1}^{\infty}\frac{(-1)^n}{2n-1}\psi(t_i) \tag{28}$$

Fig. 13 demonstrates the kinetics of line resistance change caused by a random time-dependent current and temperature set.

6. Application for system level reliability aware computing

In this section, we present a potential application of the proposed EM model for reliability-aware energy-efficient computing at the server level. We look at the KnightShift architecture [2], which is a server-level heterogeneous server architecture that introduces an active low-power mode using the additional computing node called the Knight. KnightShift enables two energy-efficient operating regions from two different CPUs. Fig. 14 shows the power trace a KnightShift architecture will generate, where the Knight is a node with a 1.8 GHz Intel Atom D525, which operates from 15W to 16.7W, and the CPU and memory consumes 9W at idle, while the primary node corresponds to dual 2.13 GHz 4-code Intel Xeon L5630 that consumes from 156W to 205W at active mode.

The main benefit of the KnightShift architecture is that the primary node can be powered off to save energy during the light demands and Knight can still operate to take the light loads. If the both power-on and

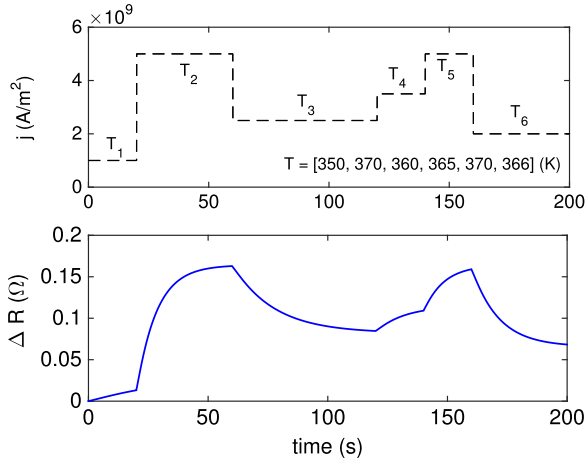

Fig. 13. Resistance evolution caused by random time-varying current densities and temperatures.

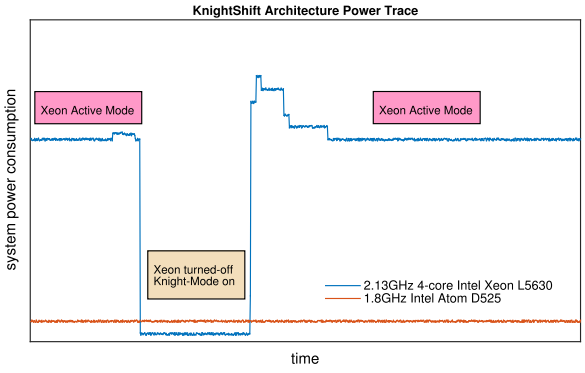

Fig. 14. Power trace in KnightShift server [2].

shut-down time can be properly managed and controlled such that performance can still be maintained, then we can significantly extend the server reliability by leveraging the EM recovery effects, predicted by the proposed model. Note that KnightShift can also place the primary server in suspend mode quicker than shutting down, but at the cost of higher idle power. For the sake of illustration, we only consider the shut-down situation in this work.

Specifically, we present two different power traces for the Xeon CPU based on [23] for our analysis. As demonstrated in Fig. 15(a), the two traces are different in that the Xeon CPU is working during t_a and t_b in *case*1 and is turned-off in *case*2. The temperature is assumed to be 363 K when Xeon node is active and 340 K when it is off [24]. During this period (t_a and t_b), the task loads could be taken over by the Knight node when the demand is light, or by other primary node in a server cluster for heavy demands. Such power-off period not only leads to energy saving, it also can be served as the recovery period for EM effect to extend the lifetime of the chip. Indeed, by using the proposed EM model, we find that the interconnect lifetime in *case*2 can be extended to be 42% longer than that of *case*1 due to EM recovery during t_a and t_b as shown in Fig. 15(b). For each CPU, if we can extend the power-off periods even longer or reduce the power-on periods while still maintain the performance requirement, we can achieve both energy saving and much longer lifetime (even immortal EM-induced life). As a result, the new EM recovery model can lead to more opportunities for system level

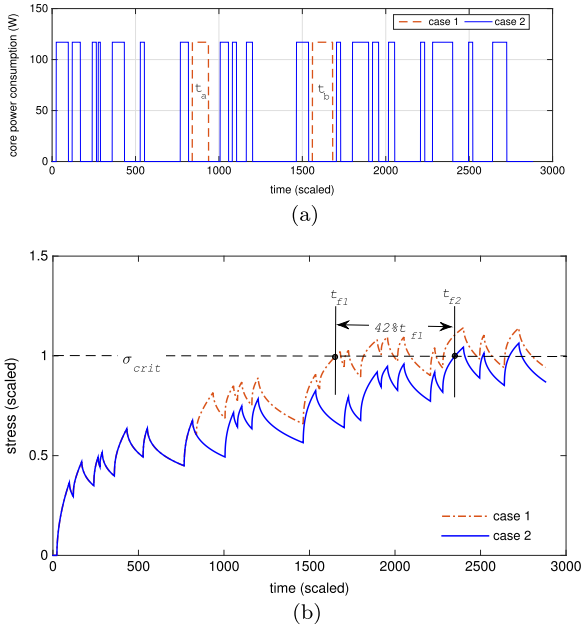

Fig. 15. (a) Two cases of the power trace for Xeon node and (b) the resulting hydrostatic stress evolution kinetics in the interconnect, where current density is assumed to be 4×10^9 A/m^2.

reliability optimization or combined energy and reliability management and optimization.

7. Conclusion

In this article, we proposed the new model for EM-induced degradation, which for the first time accounts for the transient stress recovery effect. Nowadays the recovery effect becomes more significant and relevant due to available low power and energy optimization and management techniques at multiple system levels. The new dynamic model is based on the direct analytical solution of Korhonen's equation with arbitrary unipolar or bipolar current loads at varying temperatures. We have demonstrated that the recovery effect can be quite significant even under time-dependent unidirectional current loads. Large difference in current densities and high temperature during the healing process will lead to a more complete recovery. Such effect can be further leveraged to extend the lifetime of the on-chip interconnect if the driving powers will be properly controlled and managed at the run time. Our numerical results show that the results generated by the proposed analytical model agree well with the numerical analysis results under any time-varying current densities and temperature profiles. Potential applications of the proposed model have been demonstrated.

References

[1] B. Bailey, Thermally challenged, in: Semiconductor Engineering, 2013.

[2] D. Wong, M. Annavaram, KnightShift: scaling the energy proportionality wall through server-level heterogeneity, in: 2012 45th Annual IEEE/ACM International Symposium on Microarchitecture (MICRO), 2012, pp. 119–130. http://dx.doi.org/10.1109/MICRO.2012.20.

[3] ARM big.LITTLE Technology ⟨http://www.arm.com/products/processors/technologies/biglittleprocessing.php⟩.

[4] Y.-J. Park, K.-D. Lee, W.R. Hunter, A variable current exponent model for electromigration lifetime relaxation in short Cu interconnects, in: International Electron Devices Meeting (IEDM'06), 2006, pp. 1–4.

[5] K. Hinode, T. Furusawa, Y. Homma, Relaxation phenomenon during electromigration under pulsed current, in: IEEE International Reliability Physics Symposium (IRPS), 1992, pp. 205–210.

[6] K.-D. Lee, Electromigration recovery and short lead effect under bipolar- and unipolar-pulse current, in: IEEE International Reliability Physics Symposium (IRPS), 2012, pp. 6B.3.1–6B.3.4.

[7] M.H. Lin, A.S. Oates, AC and pulsed-DC stress electromigration failure mechanisms in Cu interconnects, in: Proceedings of the International Interconnect Technology Conference (IITC), 2013, pp. 1–3.

[8] H. Esmaeilzadeh, E. Blem, R. St Amant, K. Sankaralingam, D. Burger, Dark silicon and the end of multicore scaling, IEEE Micro 32 (3) (2012) 122–134.

[9] V. Sukharev, X. Huang, S.X.-D. Tan, Electromigration induced stress evolution under alternate current and pulse current loads, J. Appl. Phys. 118 (2015) 034504-1–034504-10.

[10] J.R. Black, Electromigration—a brief survey and some recent results, IEEE Trans. Electron Devices 16 (4) (1969) 338–347.

[11] B.-K. Liew, N.W. Cheung, C. Hu, Projecting interconnect electromigration lifetime for arbitrary current waveforms, IEEE Trans. Electron Devices 37 (5) (1990) 1343–1351.

[12] W.R. Hunter, Self-consistent solutions for allowed interconnect current density, IEEE Trans. Electron Devices 44 (2) (1997) 304–316.

[13] Z. Lu, W. Huang, J. Lach, M. Stan, K. Skadron, Interconnect lifetime prediction under dynamic stress for reliability-aware design, in: Proceedings of the International Conference on Computer Aided Design (ICCAD), 2004, pp. 327–334.

[14] H. Chen, S.X.-D. Tan, X. Huang, V. Sukharev, New electromigration modeling and analysis considering time-varying temperature and current densities, in: Proceedings of the Asia South Pacific Design Automation Conference (ASPDAC), 2015.

[15] M.A. Korhonen, P. Borgesen, K.N. Tu, C.Y. Li, Stress evolution due to electromigration in confined metal lines, J. Appl. Phys. 73 (8) (1993) 3790–3799.

[16] V. Sukharev, Beyond Black's equation: full-chip EM/SM assessment in 3D IC stack, Microelectron. Eng. 120 (2014) 99–105.

[17] X. Huang, T. Yu, V. Sukharev, S.X.-D. Tan, Physics-based electromigration assessment for power grid networks, in: Proceedings of the Design Automation Conference (DAC), 2014, pp. 1–6.

[18] Comsol multiphysics ⟨http://www.comsol.com⟩.

[19] Failure Mechanisms and Models for Semiconductor Devices, in: JEDEC Publication JEP122-A, Jedec Solid State Technology Association, 2002.

[20] I.A. Blech, Electromigration in thin aluminum films on titanium nitride, J. Appl. Phys. 47 (4) (1976) 1203–1208.

[21] S. Chatterjee, M.B. Fawaz, F.N. Najm, Redundancy-aware electromigration checking for mesh power grids, in: Proceedings of the International Conference on Computer Aided Design (ICCAD), 2013, pp. 540–547.

[22] R. Monig, R.R. Keller, C.A. Volkert, Thermal fatigue testing of thin metal films, Rev. Sci. Instrum. 75 (11) (2004) 4997–5004.

[23] B.-G. Chun, G. Iannaccone, G. Iannaccone, R. Katz, G. Lee, L. Niccolini, An energy case for hybrid datacenters, SIGOPS Oper. Syst. Rev. 44 (1) (2010) 76–80.

[24] D. Shin, J. Kim, N. Chang, J. Choi, S.W. Chung, E.-Y. Chung, Energy-optimal dynamic thermal management for Green computing, in: Proceedings of the International Conference on Computer Aided Design (ICCAD), 2009, pp. 652–657.